https://doi.org/10.5194/egusphere-2026-5371
Preprint. Discussion started: 25 September 2026

Interannual variations and future changes in the soil uptake of hydrogen

Ye Wang*, Oliver Wild*, Xuewei Hou, Ryan Hossaini

Lancaster Environment Centre, Lancaster University, Lancaster, UK

Correspondence to: Ye Wang (y.wang251@lancaster.ac.uk), Oliver Wild (o.wild@lancaster.ac.uk)

Abstract: Hydrogen (H_2) is under consideration as a green energy source for future low-carbon development pathways. However, assessment of the future climate impacts of large-scale H_2 use is currently limited by poor understanding of the dominant atmospheric removal process, the uptake of H_2 by microbial activity in soil. Here we implement a soil dry deposition scheme for H_2 in a global chemistry transport model and conduct a sensitivity analysis to quantify how uncertainties in soil parameters contribute to uncertainty in H_2 uptake. We find that soil moisture dominates the uncertainty (52 %), along with contributions from soil porosity (34 %) and the water threshold for biological activity (13 %). However, the sensitivity of uptake to soil moisture is strongly nonlinear, with increases in uptake with declining soil moisture where it is under biotic control and with increasing soil moisture where it is under diffusivity control. We show that soil uptake dominates the interannual variation in atmospheric H_2 abundance from 2010 to 2022, and the notable decrease in 2015, while enhanced atmospheric production drives the observed long-term increase. Our results suggest that both soil sink and source of H_2 are affected by strong ENSO events driven by changes in soil moisture. Using output from 11 CMIP6 models, we project changes in H_2 soil uptake between 2015 and 2100 of −2.5 % to +7.9 % under SSP1-2.6 and +4.1 % to +20.4 % under SSP5-8.5, suggesting an increase in soil uptake under climate change associated with future changes in soil moisture.

https://doi.org/10.5194/egusphere-2026-5371
Preprint. Discussion started: 25 September 2026

1. Introduction

Hydrogen (H_2) is the second most abundant oxidizable trace gas in the troposphere *(Ehhalt and Rohrer, 2009)*, and currently has a global average mixing ratio of approximately 530 parts per billion (ppb) *(Novelli et al., 1999; Patterson et al., 2020)*. The dominant photochemical sink of H_2 in the troposphere is reaction with hydroxyl radicals (OH). However, reaction with OH is also the major atmospheric sink for methane (CH_4), and hence an increase in H_2 concentrations leads to a longer lifetime and a higher atmospheric abundance of CH_4 *(Bryant et al., 2024; Derwent et al., 2001; Derwent et al., 2020; Field and Derwent, 2021; Warwick et al., 2004)*. This causes increased production of the greenhouse gas ozone (O_3), and affects the formation of a wide range of tropospheric trace gases and aerosol *(O'Connor et al., 2022)*. In the stratosphere, the oxidation of hydrogen and methane lead to elevated levels of stratospheric water vapor, which may have significant implications for climate and stratospheric O_3 *(Tromp et al., 2003; Warwick et al., 2004)*. Moreover, increases in atmospheric hydrogen affect the recovery of stratospheric O_3 by increasing the production of HO_x radicals (i.e., OH and HO_2), which play a role in O_3 destruction *(Warwick et al., 2023)*. As a result, changes in H_2 abundance cause a range of indirect climate impacts though the troposphere and stratosphere. The 100-year global warming potential (GWP100) of H_2 is estimated to be 11.6±2.8 *(Sand et al., 2023)*, although a recent study adjusting OH concentrations to match the observationally-derived CH_4 chemical lifetime suggests a 20% lower estimate of 8.8 *(Yang et al., 2025)*.

Observations at background sites suggest that global average surface H_2 mixing ratios increased by about 1.4±0.7 ppb yr^{-1} between 2010 and 2019 because of increased H_2 industrial and leakage sources *(Paulot et al., 2024)*. In a future low-carbon economy, widespread usage of H_2 is considered a promising alternative as an energy carrier to fulfil increasing energy demand while replacing fossil fuel use. Over recent years, there has been increased interest and investment in H_2 worldwide *(International Energy Agency, 2024)*, resulting in enhanced H_2 demand. Global H_2 demand was almost 100 Mt yr^{-1} in 2024 and is predicted to reach 402–660 Mt yr^{-1} by 2050 *(Trapani et al., 2025)*. Along with the increasing demand for H_2, leakages across the supply chain are projected to rise from 1.3 Mt yr^{-1} in 2023 to 22.0–45.3 Mt yr^{-1} in 2050. Such a dramatic increase in leakage raises concerns about the future climate impacts of increased H_2 concentrations, and thus good understanding of the atmospheric H_2 budget is very important.

The tropospheric H_2 abundance is dominated by four processes: surface emissions, atmospheric production, atmospheric loss, and the soil sink. Photolysis of formaldehyde (HCHO) is the main photochemical source of H_2, and this exceeds direct anthropogenic sources from fossil fuel combustion and leakage. Reaction with OH is the main photochemical sink of H_2, but this is less important than uptake by microbial activity in soil, which accounts for 70–80 % of the total loss. A recent assessment of the H_2 budget for 2010 based on an ensemble of atmospheric models found sources from chemical production (47 Tg yr^{-1}) and emissions (36 Tg yr^{-1}) balanced by sinks to photochemistry (25 Tg yr^{-1}) and soil uptake (57 Tg yr^{-1}) *(Sand et al., 2023)*. Another study estimated an annual average sink of H_2 of 68.4 Tg yr^{-1} during 2010–2020, with soil uptake accounting for 73 % of this *(Ouyang et al., 2025)*. In contrast to the other processes, uncertainty in assessment of the soil sink of H_2 remains high because of limited understanding of the governing biological processes *(Paulot et al., 2021)*.

Soil uptake of H_2 is typically represented in models through calculation of a two-layer deposition velocity *(Brown et al., 2025; Ehhalt and Rohrer, 2013; Paulot et al., 2021; Yonemura et al., 2000)*. A new, more comprehensive scheme was recently developed by *Bertagni et al. (2021)*, coupling water and hydrogen dynamics in 12 soil textures, with thresholds for estimating the deposition velocity based on the relationship between soil characteristics and soil water potential. This scheme delivers a lower H_2 soil uptake (47.2 Tg yr^{-1} averaged over 2003–2013) *(Stroo et al., 2026)* than previous estimates. The soil moisture dependence from this scheme was subsequently adopted in an existing H_2 deposition scheme *(Paulot et al., 2024)*, which was shown to represent the global trend in H_2 concentration and the latitude distribution of deposition velocities relatively well. A lower water-

https://doi.org/10.5194/egusphere-2026-5371
Preprint. Discussion started: 25 September 2026

activation threshold for the canopy and litter resistance in this scheme was shown to provide a better seasonality but greatly overestimated the hemispheric gradient.

Given the critical role of soil uptake processes in controlling the atmospheric abundance of H_2, it is important to understand the uncertainty in representation of these processes. Recent studies have focused on the range of uptake rates across different models. For instance, *Brown et al. (2025)* calculated a 20 % spread in H_2 soil uptake based on results from Coupled Model Intercomparison Project Phase 6 (CMIP6) models due to large differences in soil moisture and porosity. Parameter perturbation approaches to identify the sensitivity to different processes are computationally expensive and impractical for complex models, but Gaussian process emulation approaches have been successfully applied to address this *(Ryan et al., 2018; Wild and Ryan, 2026)*. *Wild and Ryan (2026)* used Gaussian process emulation with a global chemistry transport model to show that the largest contributions to uncertainty in tropospheric ozone and OH arise from photochemical parameters, and from factors controlling photolysis, which initiates tropospheric photochemistry.

Despite a sustained increase since 2010, the observed atmospheric H_2 abundance exhibited an unexpected drop during 2014–2015 (Fig. A1). The causes of this interannual variability remain poorly quantified, even though several studies have reproduced the overall trend. *Paulot et al. (2024)* simulated H_2 concentrations from 2010 to 2019, and suggested that the failure to reproduce the observed increase in H_2 concentrations at background sites could be attributed to underestimation of current anthropogenic emissions, including potential leakages from H_2-producing facilities. *Surawski et al. (2026)* performed a long-term budget simulation and reproduced the upward trend in observed H_2 from 2010 to 2023. *Brown et al. (2026)* implemented H_2 emissions and an H_2 soil uptake scheme into the UK Earth System Model and showed that the model captures long-term trends from the pre-industrial to 2012, and reproduces the observed seasonal cycles of both H_2 and CH_4. A recent H_2 inversion study from *Stroo et al. (2026)* suggested that the growth of H_2 between 2003–2023 was primarily driven by changes in the photochemical source from CH_4 oxidation, together with a declining global soil sink. However, the role of soil uptake in interannual H_2 variability in recent years is not well understood and remains a significant research gap.

The analytical results of *Bertagni et al. (2021)* suggest that H_2 diffusion through the soil generally limits H_2 uptake in humid regions, while biotic limitations occur in hyperarid soils where bacteria suffer from a lack of water. However, this was based on analysis of a single year, and variation in long-term historical H_2 dry deposition velocity and its sensitivity to soil parameters has not been fully explored. The influence of intense climate events such as El Niño on H_2 soil uptake also remains unclear. Using CMIP6 output data from five models with a two-layer deposition scheme, *Brown et al. (2025)* showed changes in global mean deposition velocity from 2015 to 2100 under a range of climate scenarios. Results indicated that the deposition velocity increased by 4.8 % under the SSP1-2.6 scenario between 2015 and 2100 and by 16.7 % under SSP5-8.5. However, they focused on quantifying the spread of future deposition velocities from different models and assessing inter-model uncertainty, while the mechanisms underlying these projected increases remain poorly understood.

This study provides an assessment of the overall uncertainty in H_2 soil deposition velocity from major soil parameters, quantifies the contribution of the soil sink to interannual variation in tropospheric H_2 abundance, and projects the future H_2 soil uptake from 2015 to 2100. We introduce the atmospheric model, soil deposition scheme, and soil parameter data in Sect. 2. We compare the simulated H_2 deposition velocity, tropospheric budget, and surface mixing ratios with observations in Sects. 3.1 and 3.2. We quantify the uncertainty in deposition from different soil factors in Sect. 3.3. We then diagnose the spatial and temporal sensitivity of soil deposition velocity to soil moisture in Sect. 3.4, allowing us to explain the changes in velocity from 2010 to 2022. We further explore the role of the soil sink in the interannual variation in H_2 abundance in Sect. 3.5, and project the changes H_2 soil deposition under different future scenarios in Sect. 3.6. We present our conclusions in Sect. 4.

https://doi.org/10.5194/egusphere-2026-5371
Preprint. Discussion started: 25 September 2026

2. Data, model, and methods

2.1 Global chemical transport model

To simulate the global atmospheric H_2 budget we use the Frontier Research System for Global Change version of the University of California Irvine Chemical Transport Model (FRSGC/UCI CTM) as described in *Wild (2007)*. This model was developed to represent gas-phase processes and was run at T42 (2.8° × 2.8°) horizontal resolution with 57 vertical levels between the surface and 64 km driven by meteorological fields from the European Centre for Medium-Range Weather Forecasts (ECMWF) Integrated Forecast System (IFS). We use an updated version of the model that includes iodine chemistry. We have also expanded the treatment of volatile organic compounds to include acetone and methanol chemistry, as these influence the abundance of HCHO which is important as a source of H_2.

Anthropogenic emissions of CO, NO, and VOC species were taken from the Copernicus Atmosphere Monitoring Service global emissions (CAMS-GLOB-ANTH) v6.2 emission inventory, while biogenic emissions were from the CAMS-GLOB-BIO dataset. Soil emissions of NO_x were from CAMS-GLOB-SOIL v2.4. Biomass burning emissions for species including H_2 were taken from the CAMS Global Fire Assimilation System (GFAS) v1.2. We estimated H_2 anthropogenic emissions from combustion sources using CO-based emission factors (H_2/CO) from *Paulot et al. (2021)* for the relevant emission sectors. The oceanic source of H_2 was taken to be 6.0 Tg yr^{-1} following previous studies *(Ehhalt and Rohrer, 2009; Price et al., 2007; Rhee et al., 2006; Yashiro et al., 2011)*, and distributed based on oceanic emissions of CO from the POET inventory *(Granier et al., 2005)*. Soil emissions are assumed to be 4.5 Tg yr^{-1}, following *Paulot et al. (2024)*, and are distributed according to NO_x soil emission. We assume a H_2 leakage rate of 2.0 % each year, taking total H_2 demand from the Global Hydrogen Review 2024 *(International Energy Agency, 2024)*, and distribute this based on transportation CO emissions. To avoid double-counting, agricultural waste burning has been removed from the anthropogenic source, as this sector is already included in GFAS. Overall, annual H_2 emissions are higher in the Northern Hemisphere than in the Southern Hemisphere, with anthropogenic sources dominating in the former and biomass burning in the latter (Fig. S1).

Fig. 1 shows the global total annual emissions of H_2 from anthropogenic (energy, industry, residential and commercial buildings, transportation, waste, ships, and leakage), natural (soil and oceanic), and biomass burning sources based on the above estimates during 2010–2022. As variations in anthropogenic and biomass burning emissions are the primary contributor to the annual variation in H_2 emissions, we show these separately in Fig. 1. Transportation dominates anthropogenic sources, with emissions from industrial, residential, and leakage also playing important roles. Driven by high anthropogenic (14.5 Tg) and biomass burning (9.0 Tg) emissions in 2015, H_2 total emission peaked at 33.9 Tg yr^{-1} and then decreased to 29.2 Tg yr^{-1} in 2022. Our estimates are lower than those of *Paulot et al. (2024)* due to lower anthropogenic CO emissions and biomass burning from the inventories we are using, but fall within the range of 27−68 Tg yr^{-1} in 2010 from *Sand et al. (2023)*, and align well with the emissions of 31.5 Tg yr^{-1} averaged over 2010−2020 from the recent H_2 budget assessment of *Ouyang et al. (2025)*.

https://doi.org/10.5194/egusphere-2026-5371
Preprint. Discussion started: 25 September 2026

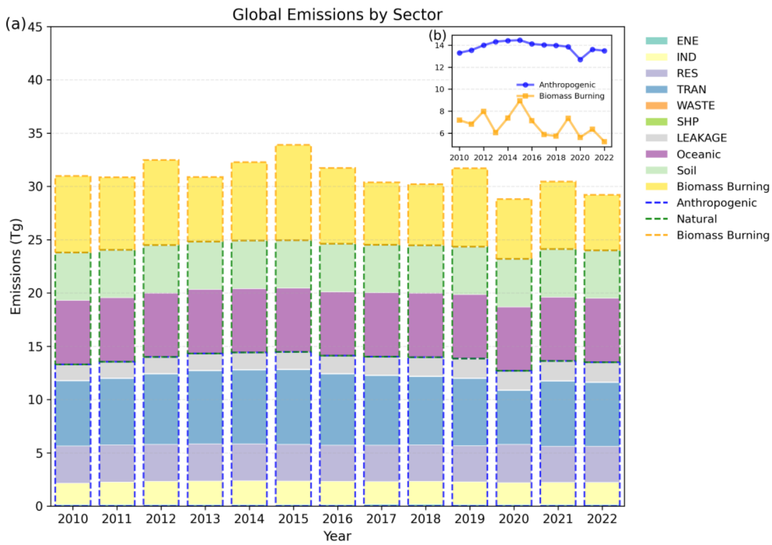

Figure 1. H_2 emissions from different sources from 2010 to 2022. Anthropogenic, natural, and biomass burning sources are outlined separately with blue, green, and orange dashed lines, respectively. Variations in anthropogenic and biomass burning emissions from 2010 to 2022 are shown in the inset in the upper righthand corner.

The standard control experiment (CTRL) simulates the variation in H_2 concentration and associated budgets from 2010 to 2017 under varying meteorology, including interannually varying anthropogenic, biomass-burning, and natural emissions. We extend these runs from 2018 to 2022 using varying emissions but holding meteorological conditions fixed at 2017 as we do not have a consistent set of meteorological fields for the following years. We impose annual mean latitudinally-varying atmospheric mixing ratios for CH_4 following CMIP6 recommendations, extending these beyond 2015 using NOAA annual mean observations such that the global mean abundance of CH_4 shows an increase from 1808 ppb in 2010 to 1920 ppb in 2022. We then perform an experiment with a modified soil source to explore the influence of changes in soil emissions during 2014–2015, and a simulation with deposition velocities fixed at 2010 values to isolate the contribution of soil uptake to interannual variability in H_2 from 2010 to 2022. Simulations were started in 2008, and the first two years were used as spin-up.

2.2 Deposition velocity calculation

The deposition scheme of *Paulot et al. (2024)* was applied in this study to calculate H_2 dry deposition velocity. The deposition velocity $v_d(H_2)$ can be expressed as:

$$\frac{1}{v_d(H_2)} = \frac{1}{g_i} + \frac{1}{g_s}$$

where g_i represents the H_2 conductance through an inactive surface layer of litter or snow and g_s represents the conductance in the soil. The latter is expressed following *Ehhalt and Rohrer (2013)* as

$$g_s = \sqrt{k_m h(T) f D_s}$$

https://doi.org/10.5194/egusphere-2026-5371
Preprint. Discussion started: 25 September 2026

where $h(T)$ and f are the sensitivity of H_2 biological uptake to soil temperature and soil moisture, respectively. We show the function of $h(T)$ and f for Sand and Loam soil types in Fig. S2. D_s is the moisture-dependent diffusivity of H_2 in the soil. k_m represents the maximum uptake rate of H_2 and is used to constrain the annual mean deposition velocity over land to a reference value of 0.035 cm s^{-1}. Moisture dependencies were calculated following *Bertagni et al. (2021)* as

$$\frac{D_s}{D_0} = \alpha_1 n^{\alpha_2}(1 - s)^{\alpha_3}$$

where D_0 (cm^2 s^{-1}) is the free air diffusion coefficient suggested by *Ehhalt and Rohrer (2013)*, and the values for α_1, α_2, α_3 are assigned to be 1, 2, and $2 + 3/b$. Here n and b have specific values for different soil textures (see Table S1 and *Bertagni et al. (2021)* for details). Further details of the calculation of f are given in the Supplement.

When regions are covered by snow, $g_i = g_{snow}$, and this is calculated from snow depth assuming a snow porosity of 0.645, following *Pinzer et al. (2010)*. The standard scheme (S1) neglects canopy and litter resistances. We therefore additionally explore an alternative scheme (S2), which accounts for canopy and litter conductance and adopts a lower water-activation threshold (–10000 kPa). A comparison of the soil moisture thresholds for different soil types supporting biological activity for the standard (–3000 kPa) and the lower (–10000 kPa) water-activation thresholds is provided in Table S1. Based on the study of *Makar et al. (2018)*, the canopy resistance was assigned specific values for different vegetation types. The litter conductance is estimated assuming a litter porosity of 0.62 *(Wang et al., 2019)*. The litter depth is estimated from simulated above-ground carbon from the IPSL Interaction with Chemistry and Aerosols (INCA) model historical simulation *(Boucher et al., 2018)*, assuming a density of 0.03 g cm^{-3}. When we apply scheme S2, k_m is used to adjust the value of annual land mean deposition velocity in 2010 to be the same as that calculated based on the standard scheme (we apply 0.185 for the standard scheme and 0.30 for the alternative scheme). We use the soil parameters described in Sect. 2.3 below to drive an offline calculation of H_2 deposition velocity, and apply the resulting deposition velocity in the CTM to calculate the dry deposition of H_2.

2.3 Soil parameters

For historical estimation, we use parameters of soil texture, soil porosity, surface atmospheric pressure, snow depth, upper 10 cm soil temperature and soil moisture content from the Global Land Data Assimilation System, GLDAS (https://disc.gsfc.nasa.gov/datasets?keywords=GLDAS) Noah v2.1, with a horizontal resolution of 1.0° × 1.0°. We adopt monthly parameters for calculation of deposition velocities, with invariant values for soil texture and porosity. The soil moisture content (kg m^{-2}) is converted to soil volumetric water content (cm^3 cm^{-3}) using water density in the upper 10 cm.

Table 1. CMIP6 models and soil parameters selected to project future H_2 deposition velocity.

Models	Soil moisture content (kg m^{-2})	Soil temperature (K)	Snow depth (m)
ACCESS-CM2	✓	✓	-
BCC-CSM2-MR	✓	✓	✓
CanESM5	✓	✓	✓
CMCC-ESM2	✓	✓	✓
CNRM-CM6-1	✓	✓	✓
EC-Earth3-Veg-LR	✓	✓	✓

https://doi.org/10.5194/egusphere-2026-5371
Preprint. Discussion started: 25 September 2026

FGOALS-g3	✓	✓	✓
FIO-ESM-2-0	✓	-	-
GFDL-ESM4	✓	✓	✓
GISS-E2-1-G	✓	-	-
IPSL-CM6A-LR	✓	✓	✓
KACE-1-0-G	✓	✓	-
MIROC6	✓	✓	✓
MPI-ESM1-2-HR	✓	✓	-
MRI-ESM2-0	✓	✓	✓
UKESM1-0-LL	✓	✓	✓

For future projections of H_2 deposition velocity we applied monthly upper 10 cm soil moisture content, soil temperature, and snow depth outputs from selected models contributing to CMIP6 under different climate pathways (see Table 1), assuming that soil texture and porosity remained unchanged at 2015 levels. The CMIP6 models used by *Cook et al. (2020)* for drought projections were adopted as an initial reference set, as drought projections provide a useful reference for evaluating future soil moisture changes. We then selected models for which as many of the required variables as possible were available. The SSP1-2.6 and SSP5-8.5 pathways are chosen to represent scenarios with moderate and extreme climate responses, respectively. Parameter-specific trends were calculated using all available outputs (16 for soil moisture content, 14 for soil temperature, and 11 for snow depth). We employed the multi-model median rather than the mean to characterize trends because it is less influenced by outliers with unusually strong or weak trends, and this is particularly important for hydrological variables which commonly exhibit large inter-model variability. Future H_2 deposition velocity was projected individually for the 11 CMIP6 models that included outputs for all three required parameters. To maintain consistency with the GLDAS data, parameters from CMIP6 models were regridded to 1.0° × 1.0° and restricted to regions north of 60° S before trend calculation and deposition velocity estimation. Soil temperature in the upper 10 cm was calculated as a depth-weighted average, when the upper 10 cm soil moisture is available.

3. Results

3.1 Evaluation of H_2 deposition velocity

Fig. 2 shows the spatial distribution of calculated H_2 deposition velocity and a comparison against observed deposition velocities at three selected sites. The zonal mean deposition velocity shows highest soil uptake in the Northern Hemisphere, reaching a peak of 0.021 cm s^{-1} at 30–40 °N, and the mean velocity over land is 0.035 cm s^{-1}, which agrees with previous estimates: 0.033 cm s^{-1} (global average over land during 1997–2005) from *Yashiro et al. (2011)*, 0.035 cm s^{-1} (1989–2014) from *Paulot et al. (2021)*, and lower than the 0.041 cm s^{-1} (multi-model mean over 2005–2014) from *Brown et al. (2025)*. Compared to two-layer schemes, the updated moisture thresholds for different land types supporting biological activity represent the observed high uptake in dry regions better *(Jordaan et al., 2020; Smith-Downey et al., 2006)*.

Table 2. Site information for the H_2 deposition velocity observations used in this study.

Site	Location	Land type	Observation period	References
Havard Forest	42.54° N, −72.17° E	Forest	Dec 2010–Dec 2011	*Meredith et al. (2017)*
Helsinki	60.2° N, 25.5° E	Forest	Sep 2005–March 2007	*Lallo et al. (2008)*

https://doi.org/10.5194/egusphere-2026-5371
Preprint. Discussion started: 25 September 2026

Heidelberg	49.40° N, 8.70° E	Semi-urban	Jan 2005–July 2007	*Hammer and Levin (2009)*

We evaluate the calculated dry deposition velocities against observations from three sites, Harvard Forest, Helsinki, and Heidelberg, that span a range of locations and vegetation types, see Table 2. Based on the availability of valid measurements, we choose a year of monthly observations in 2011 and 2006, respectively, for Havard Forest and Helsinki, and use the full observation period (2005-2007) from Heidelberg to compare with our calculations. Our deposition velocity estimates capture the monthly variations well, with a correlation coefficient (R) of 0.69, 0.65, and 0.59 for the three sites. However, the deposition velocity is underestimated during the warm season, especially at Harvard Forest and Helsinki, as reported in other studies *(Brown et al., 2025; Paulot et al., 2021; Paulot et al., 2024)*. While this may indicate a systematic bias, it may also reflect discrepancies associated with comparison of grid-cell mean estimates with point-scale observations.

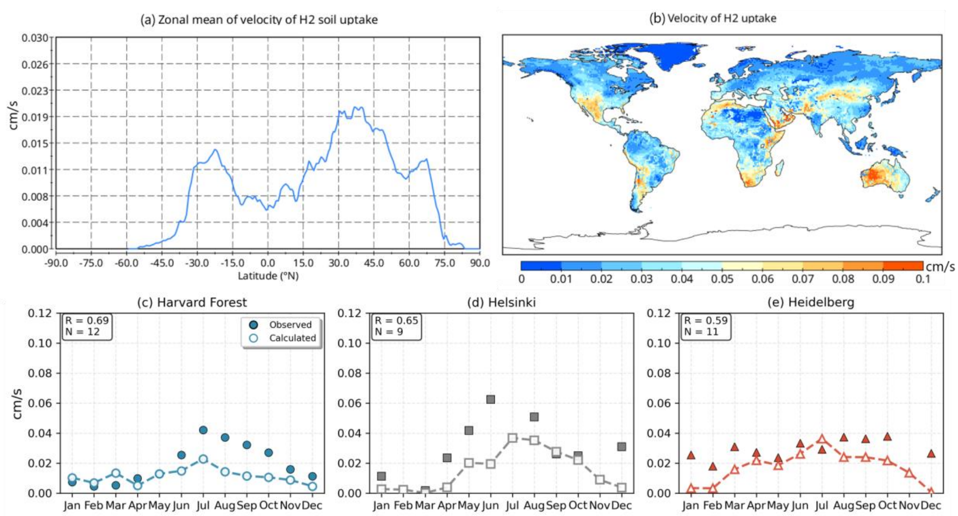

Figure 2. (a) Calculated zonal mean velocity of H_2 soil uptake, (b) distribution of velocity of H_2 soil uptake, and comparison of monthly observed (filled symbols) and calculated (2010, dashed lines) velocities at (c) Harvard Forest (2011), (c) Helsinki (2006), and (e) Heidelberg (2005–2007). See Table 2 for the locations of the observational sites.

As the magnitude and spatial distribution of H_2 deposition velocity are sensitive to the deposition scheme, we compare the results for 2010 from the two schemes described in Sect. 2.2. Applying lower thresholds for soil moisture and accounting for canopy and litter resistance (scheme S2) leads to greatly overestimated annual mean H_2 deposition velocity in 2010 over Northern Africa, the Middle East, and Southern China (see Fig. S3). The annual mean H_2 soil uptake velocity in the Middle East exceeds 0.15 cm s^{-1}, with monthly mean estimates over 0.18 cm s^{-1} in arid areas. This distribution appears less realistic, and we therefore choose the standard scheme (S1) neglecting the canopy and litter conductance for further analysis.

3.2 Evaluation of simulated H_2 budgets and concentrations

Before using the CTM to explore the changing atmospheric abundance of H_2, we evaluate the model performance in simulating current H_2 budgets and mixing ratios. Fig. 3 shows a comparison of simulated tropospheric H_2

https://doi.org/10.5194/egusphere-2026-5371
Preprint. Discussion started: 25 September 2026

burden, budgets, and lifetime, along with the CH_4 lifetime to OH, with multi-model mean results for 2010 from *Sand et al. (2023)* , and with decadal average values from 2010 to 2020 from *Ouyang et al. (2025)*. Our simulations have a longer CH_4 chemical lifetime (8.4 yrs), indicating a lower tropospheric OH burden, which in turn leads to a slightly longer H_2 atmospheric chemical lifetime of 8.0 yrs. Our estimates of H_2 atmospheric loss (23.3 Tg yr^{-1}) and atmospheric production (49.6 Tg yr^{-1}) are within the ranges reported (22–30 Tg yr^{-1} for atmospheric loss, 34–56 Tg yr^{-1} for atmospheric production). *Ouyang et al. (2025)* provides lower estimates of chemical production and loss, suggesting a lower OH abundance and consistent with the longer H_2 lifetime (2.8 yrs). Our soil sink (53.3 Tg yr^{-1}) and H_2 burden (186.6 Tg yr^{-1}) are very slightly lower than other studies but fall within the multi-model ranges, suggesting that our model performs well in simulating the emission-driven H_2 budget.

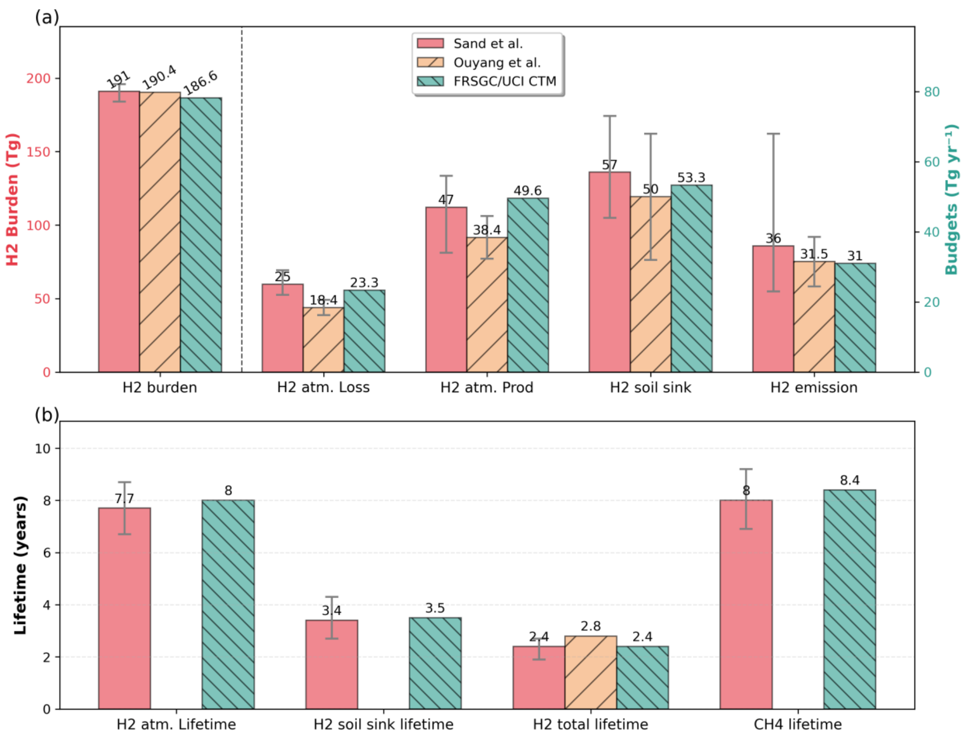

Figure 3. Comparison of simulated (a) H_2 burden (Tg) and annual flux through key production and loss processes (Tg yr^{-1}), and (b) lifetimes from the FRSGC/UCI CTM (green) with those from *Sand et al. (2023)* (red) and *Ouyang et al. (2025)* (orange). Results from *Ouyang et al. (2025)* are mean values over 2010–2020, while others are for 2010. Error bars from *Sand et al. (2023)* represent the minimum and maximum estimates across different models, and those from *Ouyang et al. (2025)* indicate one standard deviation uncertainty.

We evaluate the model performance in simulating the global distribution of H_2 using surface concentration measurements from the NOAA flask sample network *(Pétron et al., 2024)*. Spots in Fig. A1 represent the sites we selected to compare simulations with observations in 2010, which has the greatest number of sites with valid measurements, including those over the ocean. We calculate the annual mean H_2 concentration at a site only if it has at least eight valid monthly records in the year. Fig. 4a shows the observed and simulated annual mean H_2 concentrations at each site. The model successfully captures the higher H_2 concentrations observed in the Southern Hemisphere than the Northern Hemisphere, and annual mean mixing ratios are in good agreement with

https://doi.org/10.5194/egusphere-2026-5371
Preprint. Discussion started: 25 September 2026

observations. The model underestimates mixing ratios at some northern hemisphere sites, notably those at coastal sites or at high elevations where the model is unable to adequately resolve local influences on air mass origin. Statistical evaluation yields a correlation coefficient of 0.91 and a normalized mean bias of –1.7 % across annual mean samples (n=58), confirming that the model can reproduce both the north–south gradient and annual mean abundance, and can capture the observed monthly characteristics of H_2 across most sites.

Comparison of the simulated surface annual mean H_2 mixing ratios with observations at sites below 500 m altitude shows that the model can reproduce the spatial distribution of H_2 well (Fig. 4b). The north–south gradient and local characteristics over the continents are captured by the model, including high concentrations in Europe and low concentrations in the Arctic. The seasonal cycle is also well reproduced (Fig. S4), with higher H_2 in warm seasons (spring and summer). Simulated hotspots at high latitudes with extremely high H_2 concentrations in summer are attributed to intense biomass burning emissions. Overall, the model successfully captures the spatial, seasonal, monthly, and annual mean features of observed H_2 in 2010.

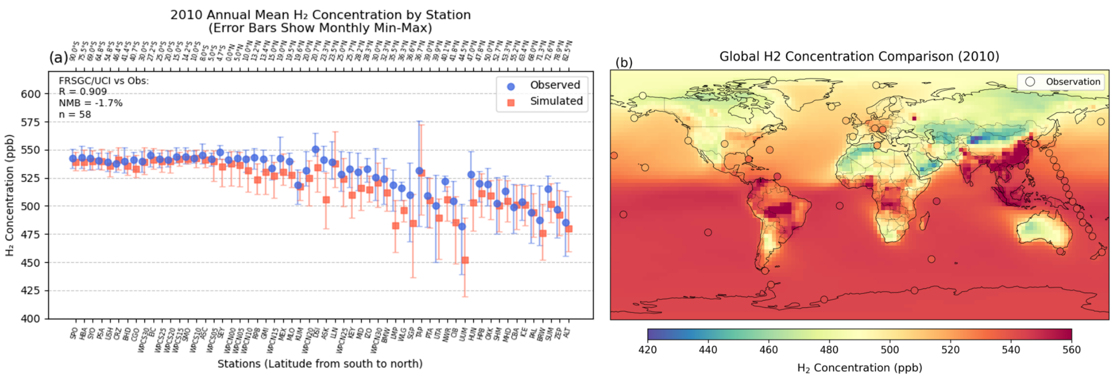

Figure 4. Comparison of simulated H_2 mixing ratios with observations in 2010. (a) annual mean H_2 mixing ratios from NOAA observation (blue) and the model (orange) with bars showing maximum and minimum monthly H_2 mixing ratios over the annual cycle. The correlation coefficient and normalised mean bias are shown in the top lefthand corner. (b) Comparison of the annual mean distribution of H_2 (shading) with observations (spots).

3.3 Quantifying uncertainty in the soil uptake of H_2

The uptake of H_2 by soil is the largest term in the atmospheric H_2 budget, and the least well characterized, and as such it may account for much of the bias in the model simulation of surface H_2 mixing ratios. Much of this uncertainty is associated with incomplete knowledge of the biological processes that underpin H_2 uptake, which are represented here through dependence on soil moisture, porosity, temperature and other properties. To characterize the uncertainty in soil uptake and quantify the contribution from different parameters, we conduct a global sensitivity analysis focusing on the six most important parameters governing uptake. To make this computationally efficient, we use Gaussian process (GP) emulation to emulate the uptake rates from the deposition scheme and then apply a Monte Carlo approach using the emulator to explore the full uncertainty associated with each parameter, following *Ryan et al. (2018)* and *Wild and Ryan (2026)*.

Table 3. Parameter uncertainty ranges and scaling approach.

Order	Parameter Definition	Uncertainty Range	Scaling Approach	Reference

https://doi.org/10.5194/egusphere-2026-5371
Preprint. Discussion started: 25 September 2026

1	Surface pressure (PS)	±1 %	linear (±X %)	*(Salstein et al., 2008)*
2	Soil moisture content (SM)	±25 %	linear (±X %)	*(Spennemann et al., 2020)*
3	Soil temperature (ST)	±3 K	linear (±X)	*(Gottschalck et al., 2005; Zhao et al., 2022a)*
4	Soil porosity (SP)	±20 %	linear (±X %)	*(Zhao et al., 2022b)*
5	Snow depth (SD)	±30 %	linear (±X %)	*(Qiao et al., 2022)*
6	Water threshold for biological activity (WAT)	[-10000, -3000]	logarithmic (absolute)	*(Paulot et al., 2024)*

Firstly, we estimate uncertainty ranges for the key parameters controlling the deposition velocity based on previous studies, see Table 3. For soil moisture, ±25 % is adopted from the average non-systematic error (unbRMSE = 24.9 %) reported by *Spennemann et al. (2020)*. For soil temperature, we adopt ±3.0 K, following *Gottschalck et al. (2005)*, who found considerable spread across GLDAS runs and *Zhao et al. (2022a)*, who reported a –3 °C underestimation in China. Soil porosity uncertainty was set at ±20 %, based on the study of *Zhao et al. (2022b)*, which showed differences of –0.2 to 0.6 between GLDAS and SMAP in normalized porosity. For snow depth, we estimated an uncertainty of 30 % by combining the snow-depth ranges from *Sturm et al. (1995)* with the GLDAS standard deviations for different snow classes reported by *Qiao et al. (2022)*; these are summarized in Table S2. There is relatively low uncertainty in surface atmospheric pressure, and we take a conservative estimate of ±1 % based on the study of *Salstein et al. (2008)* which suggested RMS differences between analyses and observations of around 2–3 hPa.

To fully sample the uncertainties across these six parameters, we use a maximin Latin Hypercube design to select 80 sets of parameter uncertainty values that optimally span the parameter space defined by the ranges in Table 3. Dry deposition velocities were calculated for all 80 sets of parameter uncertainties, and these were used to train a Gaussian process emulator. Deposition velocities were calculated for an additional 20 sets of parameter values to provide independent validation of the emulator. For each set, we emulate the monthly deposition velocities and then averaged them to derive the annual mean. Following *Ryan et al. (2018)*, we employ a Matérn–3/2 covariance function which can accommodate less smooth response surfaces, making it more suitable for representing physical behaviour. The skill of the emulators in representing the full model is evaluated by quantifying how well they reproduce the results of the 20 additional runs on which they were not trained. As shown in Fig. S5, the trained GP model reproduces the deposition velocity of H_2 over land well ($R^2 = 0.993$).

To quantify the contribution of uncertainty in each parameter to the overall uncertainty in deposition velocity, we applied a variance-based sensitivity analysis. We calculated sensitivity indices using the Sobol approach *(Sobol', 2001)*. The emulator enables efficient exploration of the parameter space, allowing Sobol analysis to be conducted using a large ensemble of evaluations that would be computationally prohibitive with the model. Analysis was conducted using a Saltelli sampling scheme *(Saltelli et al., 2010; Saltelli et al., 2004)* with a base sample size of 2000. We find that soil moisture accounts for 52 % of the overall uncertainty, soil porosity for 33 %, and the water threshold for 13 %. Soil temperature plays a smaller role, contributing less than 3 % (Fig. B1). There are small interactions between these parameters, but these make only a minor contribution. To assess whether emulator uncertainty could affect the sensitivity analysis, the ratio between the mean GP predictive variance and the

https://doi.org/10.5194/egusphere-2026-5371
Preprint. Discussion started: 25 September 2026

propagated output variance was evaluated. The resulting ratio (0.75 %) indicates that the output variability is dominated by parameter perturbations rather than by emulator uncertainty.

3.4 Sensitivity of H_2 soil sink to soil moisture variation

Given that soil moisture contributes the most to the overall uncertainty in H_2 uptake estimation, we explore the response of calculated H_2 deposition velocity to soil moisture alone. An increase in soil moisture content tends to decrease annual mean deposition velocity over land at most locations, with a greater decrease occurring for larger increments in soil moisture (from 10 % to 60 %), see Fig. 5. In contrast, decreasing soil moisture leads to increases in annual mean deposition velocity in most regions. However, beyond a drying of 30%, deposition velocities decrease again as the soil becomes extremely dry. This can be explained from the behaviour of the soil moisture dependence (f) (Fig. S3b). At locations with soil conditions wetter than the optimal value for the specific soil type, f decreases with rising soil moisture and increases with declining soil moisture. If the soil moisture falls below the optimal condition, f starts to decrease with decreasing soil moisture. For locations with soil moisture below the optimal value, the deposition velocity will increase as the soil gets wetter until the optimum moisture condition is exceeded.

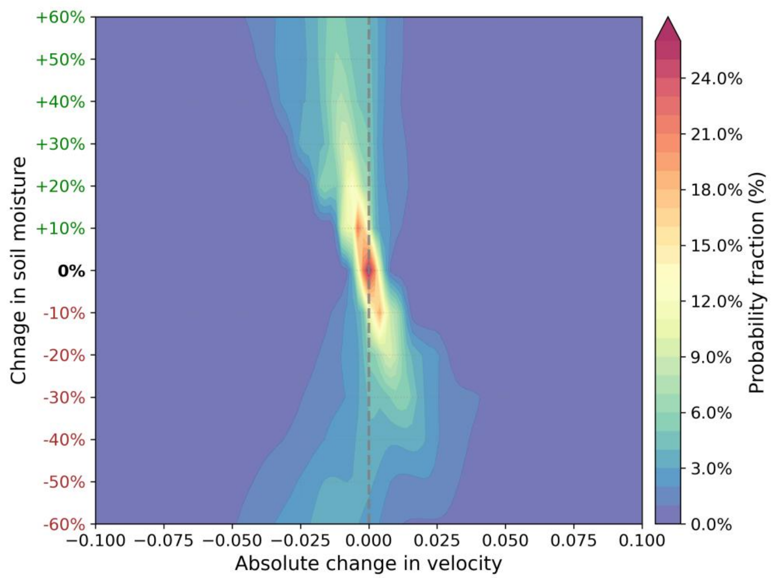

Figure 5. The probability distribution of the absolute change in dry deposition velocities (100 bins) in response to a perturbation in soil moisture content (–60 % to +60 %).

We performed a similar analysis to quantify the sensitivity of deposition velocities to soil temperature alone. We find that the response to soil temperature is much less than that to soil moisture, and that the responses are close to linear. Increasing soil temperature raises deposition velocities while decreasing soil temperature lowers them.

Regional responses of H_2 deposition velocity to soil moisture perturbations in the 2010 simulations are distinct and classifiable. Changes in H_2 dry deposition velocity exhibit opposite responses in North Africa and the Middle East to those in China, Europe and Latin America, see Fig. B2. This indicates the presence of different regimes where soil moisture affects H_2 soil uptake differently. Therefore, we explore the long-term sensitivity of H_2

https://doi.org/10.5194/egusphere-2026-5371
Preprint. Discussion started: 25 September 2026

deposition velocity to soil moisture changes during 2010–2022 by quantifying the relative contributions of diffusivity (Ds: D_s in Sect. 2.2) and biological processes (BIO: $h(T)f$ in section 2.2). The anomalies in annual mean velocity, BIO, and Ds relative to the 2010–2022 mean are shown in a quadrant plot (Fig. B3). Higher deposition velocities occur with higher Ds and BIO (purple regions in upper righthand quadrant), while lower velocities occur with lower Ds and BIO (green regions in lower lefthand quadrant). This suggests that changes in deposition velocity are driven by both Ds and BIO. BIO-driven sensitivity is indicated by purple regions in the upper lefthand quadrant, and Ds-driven sensitivity by green regions in the lower righthand quadrant. These patterns allow a classification into three regimes: BIO-dominant, Ds-dominant, and Transition zones, which correspond to sensitivity governed by BIO, Ds, or both.

Based on the three target clusters from the above analysis, an Expectation-Maximization method, Gaussian Mixture Model, was used to classify the deposition responses using gridded long-term mean BIO and Ds values as input. The Gaussian Mixture Model represents the joint distribution of BIO and Ds as a mixture of three Gaussian components and estimates the probability that each data point belongs to each component, and it has been applied to atmospheric studies to classify ozone profiles *(Fahrin et al., 2023)*, aerosol types *(Song et al., 2023)*, as well as VOC sample clusters *(Richards et al., 2020)*. Fig. 6 shows the distribution of the three sensitivity regimes characterized by thresholds of log(BIO/Ds) >1.4 (BIO dominant), log(BIO/Ds) < 0.94 (Ds dominant), and the transition regime in between. The spatial response matches the relationship between the deposition velocity and soil moisture shown in Fig. B2, with increased velocity in BIO-dominant and Transition regions under drier soil conditions and in Ds-dominant regions under wetter soil conditions The seasonal classification of these regimes is presented in Fig. S6 for January and July, and demonstrate that in winter conditions a greater number of locations are controlled by BIO processes, whereas Ds control regions expand in summer. These results align well with those of *Bertagni et al. (2021)* who presented a similar classification using different criteria. We additionally tested the sensitivity of our classification to the number of clusters selected. Using four clusters showed little obvious difference, and five clusters did not provide additional meaningful information. This suggests that three clusters is sufficient to characterise the sensitivity regimes well.

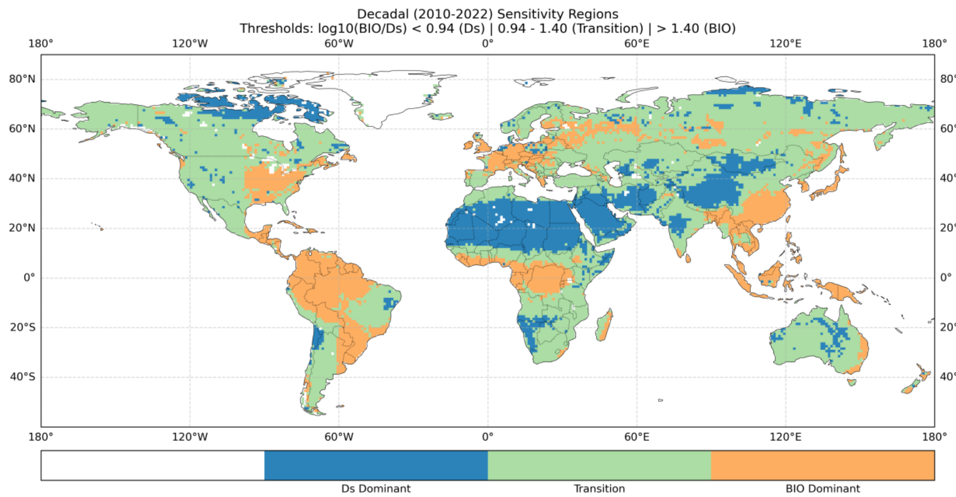

Figure 6. Identification of the sensitivity zones of H_2 deposition velocity in response to soil moisture based on H_2 soil sink processes during 2010–2022. The diffusion (Ds) dominated, Transition, and biotic (BIO) dominated regimes are indicated by blue, green, and orange, respectively, and the dynamic thresholds used to classify the regions are labelled above the figure.

https://doi.org/10.5194/egusphere-2026-5371
Preprint. Discussion started: 25 September 2026

Given the sensitivity of deposition velocity to soil moisture identified here, we examine the implications for the variations in velocity over the past decade. Fig. 7 shows the calculated annual mean dry deposition velocity over land from 2010 to 2022, along with the Niño 3.4 index that provides a measure of global climate variations. There are two pronounced peaks in deposition velocity in 2015 and 2022, and these are likely associated with strong ENSO events. Anomalies in annual mean deposition velocity and soil moisture (Fig. S7) relative to the long-term mean reveal the differing drivers for the two peaks. The 2015 peak can be attributed to drier conditions in most BIO-dominant and Transition regions, driven by El Niño, with additional contributions from increased soil moisture in northern Africa, which is Ds-dominant. In contrast, the 2022 peak reflects a combination of wetter soils in Ds-dominant regions (western China, Australia, the Middle East) and drier conditions in BIO-dominant and Transition regions (South America, eastern US, North America, Europe). The stronger signal during the 2020-2023 La Niña event compared to the 2010–2011 event is due to its longer duration, as it developed into a "triple-dip" La Niña, which cumulatively altered precipitation-induced soil moisture *(Tian et al., 2026; Zhu et al., 2025)*. We show that short-term variations in H_2 soil uptake are closely linked to strong ENSO events, which redistribute global heat and precipitation. The responses are not related in a simple linear manner due to the spatially heterogeneous climate-induced responses of soil moisture.

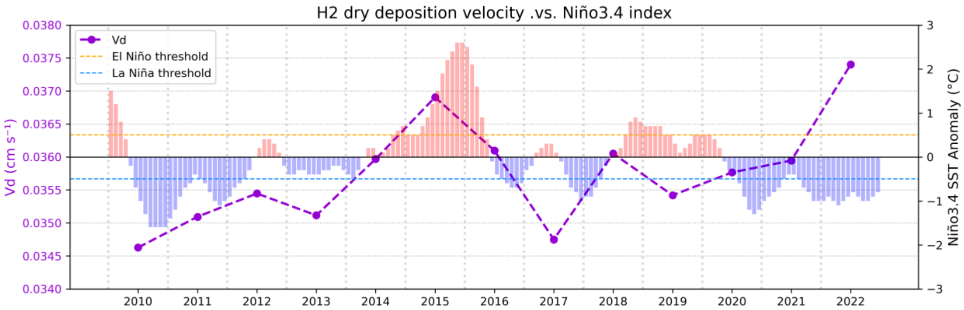

Figure 7. Time series of the annual mean H_2 dry deposition velocity over land (purple line, cm s^{-1}) and the Niño 3.4 index (bars) from 2010 to 2022. Orange and blue dashed lines represent the threshold for El Niño (+0.5 °C) and (–0.5 °C), respectively.

3.5 The contribution of H_2 dry deposition to interannual H_2 variability

Over the past decade, observed surface H_2 mixing ratios have shown an increasing trend, but with a notable drop during 2014–2015 (Fig. A1). Given that soil uptake is the largest term in the atmospheric H_2 budget, and that it is strongly dependent on soil moisture, we explore the extent to which interannual variability in soil moisture may contribute to variations in surface H_2 abundance. The anomalies in H_2 concentration at background sites relative to the 2010–2022 mean from observation and control simulation are shown in Fig. 8. We do not have self-consistent meteorological data after 2017, and we therefore simulate atmospheric transport for the 2018–2022 period using repeated meteorology from 2017, but with surface emissions and H_2 deposition velocity specific to the 2018–2022 period. The comparison suggests that the model can capture the increasing trend in H_2 abundance from 2010 to 2020 quite well, but it fails to reproduce the decline in H_2 abundance during 2014–2015.

As we have shown, the strong El Niño event during 2014–2015 had a substantial impact on soil uptake due to the soil moisture response to the climate signal. However, we assume H_2 soil emission is fixed from 2010 to 2022. H_2 emission from soil is a by-product of the nitrogenase reaction in the process of nitrogen fixation *(Flynn et al., 2014)*. The influence of hydrology on the nitrogenase reaction has been widely explored in previous studies. For example, *Kohl et al. (1991)* found that nitrogenase activity was inhibited 90 % or more as a result of drought stress.

https://doi.org/10.5194/egusphere-2026-5371
Preprint. Discussion started: 25 September 2026

Aranjuelo et al. (2011) showed a decrease in nitrogen fixation in droughted nodules, which was attributed to increased oxygen resistance. Therefore, we hypothesize that strong climate events also affect the soil emissions of H_2. To test this, we assume that drier soil conditions during 2014–2015 associated with the strong El Niño caused a decrease in H_2 soil emissions of 1.4–1.8 Tg and perform an additional model simulation (labelled "Soil-modified") to compare with our control simulation with fixed natural H_2 emissions (10.5 Tg every year). As shown in Fig. 8a, the simulation with modified soil emission captures the drop in H_2 concentration well over 2014–2015, suggesting that it would be valuable to develop an interactive soil source of H_2 which is sensitive to climate-induced soil moisture changes.

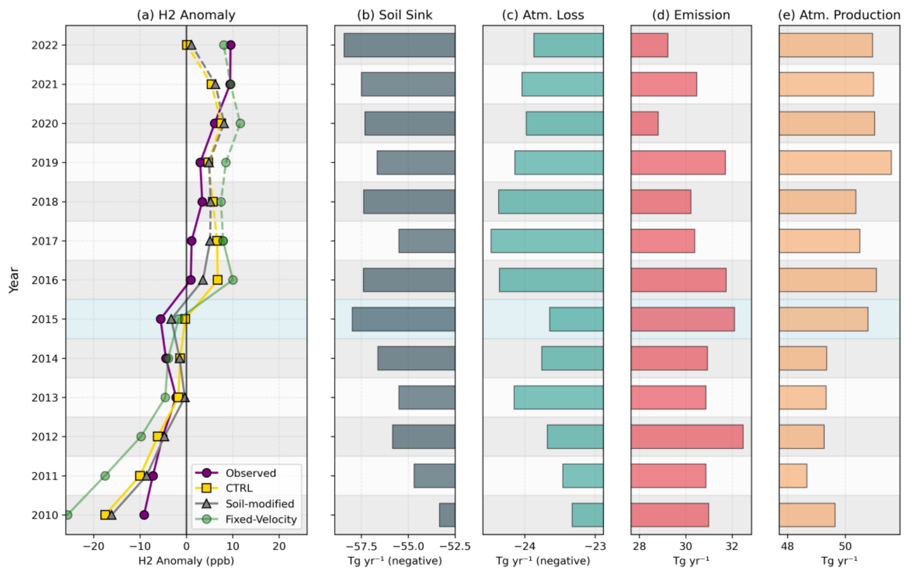

Figure 8. Anomalies of (a) annual mean H_2 mixing ratio averaged across background sites from observations (purple), CTRL (yellow), Soil-modified (grey), and Fixed-velocity (green) simulations, and annual mean H_2 budget terms from the Soil-modified simulation for (b) soil sink, (c) atmospheric loss, (d) emission, and (e) atmospheric production from 2010 to 2022. We use dashed lines to show simulated H_2 anomalies after 2017 with fixed meteorology.

To explore the role of the soil sink in governing the interannual variability in H_2, we further fixed the H_2 deposition velocity to the level of 2010, retaining the modified soil emissions during 2014–2015. This "Fixed-velocity" simulation overestimates the increase in H_2 abundance over the period and fails to reproduce the observed decline in H_2 mixing ratios during 2014–2015. This suggests that the soil sink is an important process controlling interannual variation in H_2 level over the past decade. It is clear from the tropospheric H_2 budget terms shown in Fig. 8 that the enhanced soil sink drives the drop in H_2 mixing ratio in 2015, even though emissions are high and the photochemical loss is low in this year. Similarly, the decrease in soil uptake in 2017 reduces the decline in H_2 abundance from 2016 to 2017 caused by the lower H_2 source and increased chemical loss.

The upward trend in atmospheric H_2 production, which aligns with the long-term rise in H_2 abundance, suggests that increased production is the primary factor driving the trend in abundance, which outpaces the decrease in direct emissions. This agrees with the conclusions of recent studies *(Ouyang et al., 2025; Stroo et al., 2026)*. Without the corresponding meteorology, we overestimate the decline from 2020 to 2022, suggesting that there

https://doi.org/10.5194/egusphere-2026-5371
Preprint. Discussion started: 25 September 2026

may be important meteorological impacts on chemical processes affecting H_2 during this period, especially during the long La Niña event. However, we note that there was a large decline in the observed monthly H_2 in the second half of 2022 that is captured well by the model (Fig. S8), highlighting again the important role played by the higher soil sink.

3.6 Future projection of the deposition velocity of H_2

As H_2 dry deposition is strongly influenced by soil parameters, particularly soil moisture and temperature, it is valuable to explore how soil uptake may change over the coming century under climate change. We show that future trends in soil moisture exhibit large spatial heterogeneity, whereas soil temperature and snow depth increase under both SSP1-2.6 and SSP5-8.5 pathways. Projected changes under SSP1-2.6 show similar spatial patterns to those under SSP5-8.5, but with generally smaller magnitudes. Under SSP5-8.5, the median trends range from –0.80 to 0.47 kg m^{-2} decade^{-1} for soil moisture, 0.0 to 1.68 K decade^{-1} for soil temperature, and –0.47 to 0.01 m decade^{-1} for snow depth. Future snow depth does not exhibit uniform changes across all grid cells, and regional increases in snow depth are closely linked to precipitation changes *(Fontrodona Bach et al., 2018)*. Regions with deeper snow show strong spatial consistency with areas characterized by increasing soil moisture in the future (Figs. 9a and 9c). Only 4.8 % of the land area showed robust agreement among models in soil moisture trends under the SSP1-2.6 pathway (Fig. 9a), with 36.6% agreement on SSP5-8.5 (Fig. 9d). Notably, soil conditions under the SSP5-8.5 pathway are wetter in western China, East Middle, India, central Africa, southeastern South America, while most other regions worldwide show reduced soil moisture (Fig. 9d). From the sensitivity analysis of H_2 soil sink to soil moisture change in Sect. 3.4, future increases in H_2 deposition velocity are expected as a result of decreased soil moisture in BIO-dominant or Transition regions and increases in Ds-dominant regimes, especially under the SSP5-8.5 pathway.

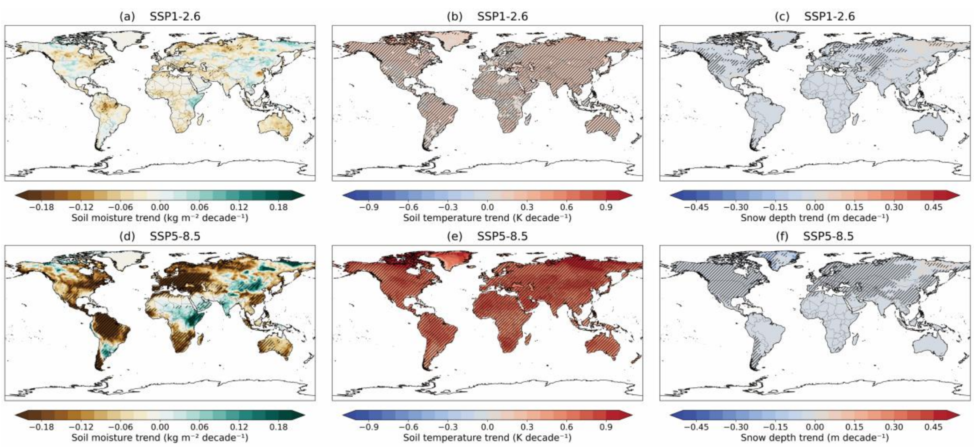

Figure 9. Median trend of upper 10 cm soil moisture (kg m^{-2} decade^{-1}), upper 10 cm soil temperature (K decade^{-1}), and snow depth (m decade^{-1}) under (a)–(c) SSP1-2.6 and (d)–(f) SSP5-8.5. The hatching on the plots indicates that nine models (for soil moisture and soil temperature), and six models (for snow depth) agree on the sign.

Fig. 10 shows the projected interannual variation in annual mean deposition velocity to land from 2015 to 2100 for each of the selected CMIP models under SSP1-2.6 and SSP5-8.5 pathways along with the percentage change between 2015 and 2100. Deposition velocities in 2015 were calculated in the range 0.018–0.040 cm s^{-1}, with more than a factor of two difference across the models driven by distinctly different levels of soil moisture.

https://doi.org/10.5194/egusphere-2026-5371
Preprint. Discussion started: 25 September 2026

Deposition velocities are projected to show relatively little change (-2.5%–7.9%) from 2015 to 2100 among models under the SSP1-2.6 pathway, although one model shows a larger increase of 7.9 %. Deposition velocities show stronger increases (4.1–20.4%) under the SSP5-8.5 pathway. The multi-model mean deposition velocity is projected to increase 0.8 % under the SSP1-2.6 pathway and 9.7 % under SSP5-8.5 between 2015 and 2100. Our projections suggest a smaller increase in H_2 deposition velocity compared to the estimates of +4.8 % for SSP1-2.6 and +16.7 % for SSP5-8.5 from *Brown et al. (2025)*, which reflects the broader selection of models we have considered and our use of soil porosity from the models, which is higher than in the GLDAS data.

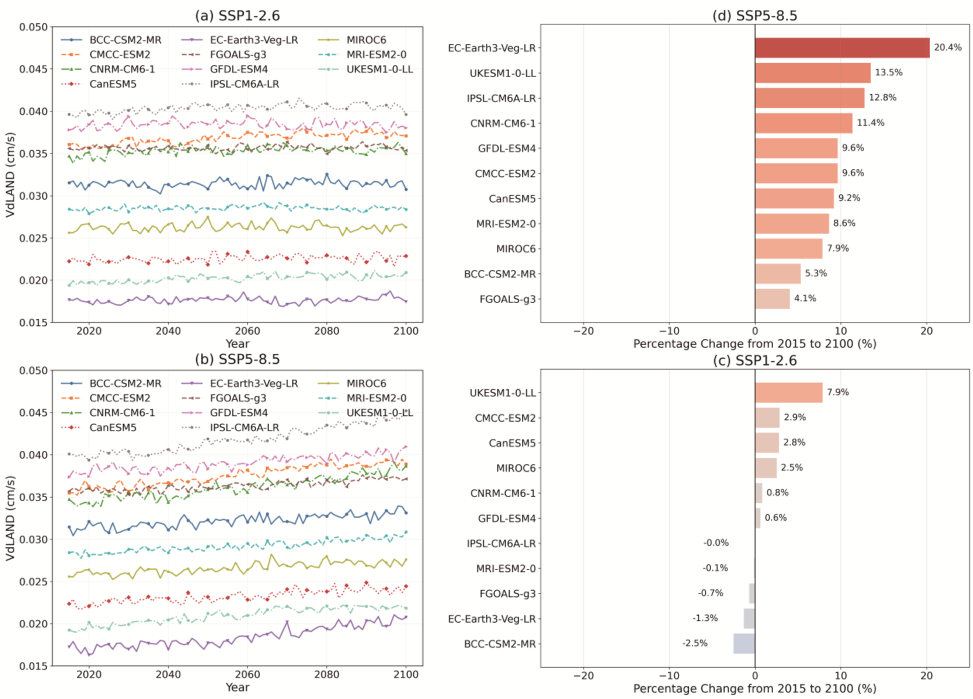

Figure 10. (a)–(b) Variations in H_2 dry deposition velocity over land from 2015 to 2100 calculated for CMIP6 models, and (c)–(d) percentage change (%) in deposition velocity between 2015 and 2100 under SSP1-2.6 and SSP5-8.5 pathways.

4. Conclusions

In this study, we have implemented a soil dry deposition scheme for H_2 in the FRSGC/UCI global chemistry transport model and have performed emission-driven simulations to investigate interannual variations and trends in H_2 from 2010 to 2022. The model reproduces the distribution and seasonality of observed surface H_2 mixing ratios and the underlying increases over the period. We find an atmospheric H_2 burden of 186.6 Tg in 2010 and an atmospheric lifetime of 2.4 years. Sources of H_2 from emissions (31.0 Tg yr^{-1}) and chemical production (49.6 Tg yr^{-1}) roughly balance losses from chemical destruction (23.3 Tg yr^{-1}) and soil uptake (53.3 Tg yr^{-1}) and these budget terms align well with those from other recent model studies. Focusing on the largest and most uncertain term in this budget, soil uptake of H_2 at the Earth's surface, we have conducted a sensitivity analysis to quantify how uncertainties in soil parameters contribute to uncertainty in H_2 uptake. We find that soil moisture dominates the uncertainty (52 %), along with contributions from soil porosity (34 %) and the water threshold for biological

https://doi.org/10.5194/egusphere-2026-5371
Preprint. Discussion started: 25 September 2026

activity (13 %). This strong sensitivity of uptake to soil moisture provides a key driver for interannual variations in atmospheric H_2 abundance and highlights the susceptibility of this important term in the H_2 budget to future changes in climate.

To explore the response of soil uptake to soil moisture we examine how update varies with global uniform changes in soil moisture. Increased soil moisture leads to lower uptake at most locations, with greater uptake at a limited number of places. Decreased soil moisture leads to greater uptake at most locations, although decreases beyond 30% cause lower uptake at an increasing number of locations, reflecting the non-linear relationships involved. To further characterize these responses in soil uptake we perform a formal classification of regional responses into biotic and diffusivity-dominated regimes, extending the approach taken by *Paulot et al. (2021)*. In the diffusivity-dominated regime, corresponding to dry soil conditions, uptake typically increases with soil moisture, and decreases with soil drying. In biotic-dominated regimes, representing conditions favourable for biological activity, uptake shows the opposite response, decreasing with soil moisture and increasing with drying. This analysis allows us to explain the complex response of soil uptake to soil moisture variations associated with ENSO events, highlighting different responses from different events associated with the spatially heterogeneous patterns of soil moisture change.

We investigate the changes in atmospheric H_2 abundance from 2010 to 2022 and find that much of the interannual variability can be explained by changes in soil uptake, particularly the drop in H_2 abundance in 2015, which cannot be reproduced with an annually invariant uptake rate. However, we are unable to fully reproduce this drop and suggest that incorporating climate-driven changes in the natural soil source of H_2 from nitrogen fixation may also be important. While soil uptake is an important driver of variability, we note that the underlying long-term increase in H_2 mixing ratios over the past decade is largely due to rising atmospheric production, as previous studies have suggested. Exploration of future changes in soil uptake using climate data from CMIP6 models over the period 2015–2100 suggests that changes in soil moisture will lead to increased uptake in future. These changes are small (averaging 0.8 %) on the SSP1-2.6 pathway but more substantial (9.7 %) on the SSP5-8.5 pathway. While this increased uptake may be sufficient to halt the increases in H_2 abundance seen over the past decade, it is unlikely to offset the increased H_2 emissions expected on many future development pathways, and it is thus essential to minimize the increased emissions expected from leakages when developing a future H_2 economy.

We have demonstrated the major contribution of the soil sink to the interannual variability in H_2 abundance, highlighting the importance of soil moisture in governing uptake and showing the impacts on recent and future H_2 abundance. However, improved understanding of microbial activity in different soil types and the role of soil moisture in governing this is needed to refine estimates of this important term in the atmospheric H_2 budget. Recent laboratory studies have identified surface litter as a strong sink of H_2, rather than simply a barrier to soil uptake as is commonly assumed *(Drewer et al., 2026)*. There is also a lack of long-term measurements of soil H_2 uptake across a diversity of biomes, and these are needed to provide a more critical test of uptake schemes. Further refinement of the atmospheric H_2 budget also requires improved estimates of the photochemical production and destruction of H_2. These terms may be overestimated in current models which typically overestimate OH, reflected in a tropospheric chemical lifetime of CH_4 of 8–9 years compared with an observationally based lifetime of 11.2±1.3 years *(Prather et al., 2012)*. Addressing this bias will increase the importance of soil uptake for atmospheric H_2 removal and emphasises the need for improved understanding.

https://doi.org/10.5194/egusphere-2026-5371
Preprint. Discussion started: 25 September 2026

Appendix A: Observation information

For each background site show in Fig. A1a, we calculated the annual mean H_2 mixing ratio only if valid measurements were available for at least eight months in that year. These site-specific annual means were averaged to obtain the multi-site annual mean for each year, and the results are shown in Fig. A1b (orange symbols), labelled with the number of sites that were included. There is a peak in 2013 (534.6 ppb), and drops in 2015 (529.0 ppb) and 2020 (536.6 ppb) during the long-term rise from 2010 to 2022. A consistent set of annual means from 13 background sites, excluding 6 sites with one or more years of missing data, are also shown in Fig. A1b (blue symbols). This smaller set shows a similar pattern, although there is a decline from 2018 to 2019 and the dip in 2020 disappears.

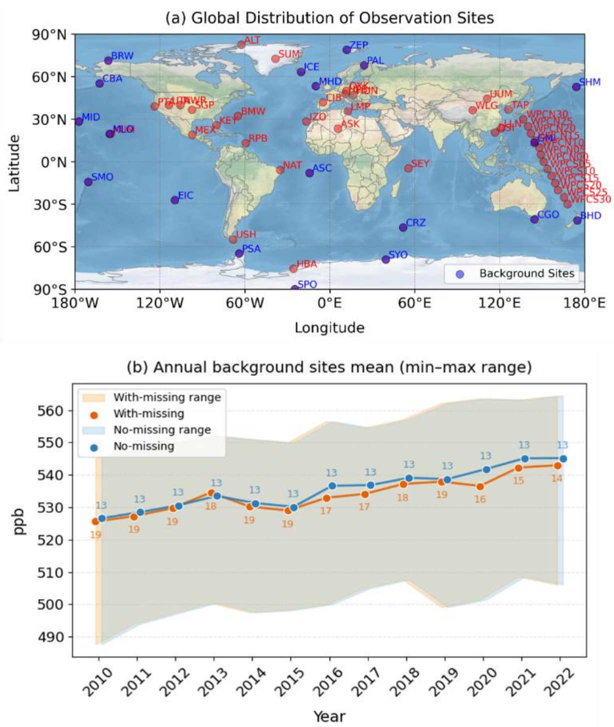

Figure A1. (a) Locations of observation sites providing H_2 measurements selected to calculate and compare with model results; blue symbols represent background sites. (b) Time series of observed annual mean H_2 mixing ratios at background sites. Orange dots: annual means with varying site counts (allowing missing data). Blue dots: annual means from consistent sites (no missing data). The background site selection follows *Paulot et al. (2024)*.

https://doi.org/10.5194/egusphere-2026-5371
Preprint. Discussion started: 25 September 2026

546 **Appendix B: Results of sensitivity analysis**

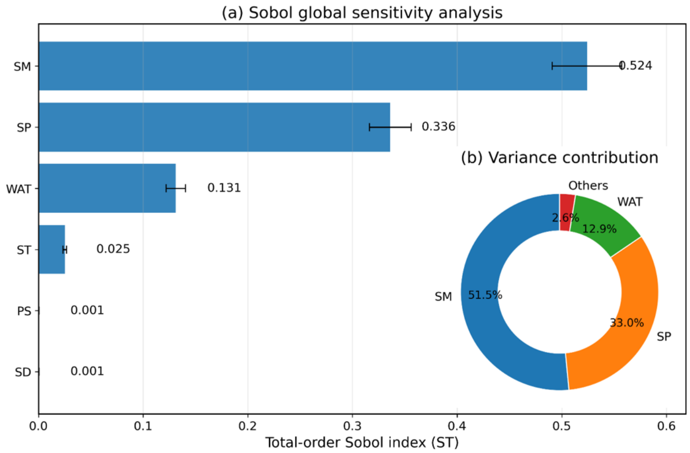

547

548 Figure B1. (a) Total-order Sobol indices showing the overall contribution of each parameter to the propagated
549 output variance, including both direct effects and parameter interactions. Error bars indicate the statistical
550 uncertainty associated with the estimated Sobol indices. (b) Percentage contributions normalized from the first-
551 order Sobol indices, representing the direct contribution of each parameter to the total output variance.

552

https://doi.org/10.5194/egusphere-2026-5371
Preprint. Discussion started: 25 September 2026

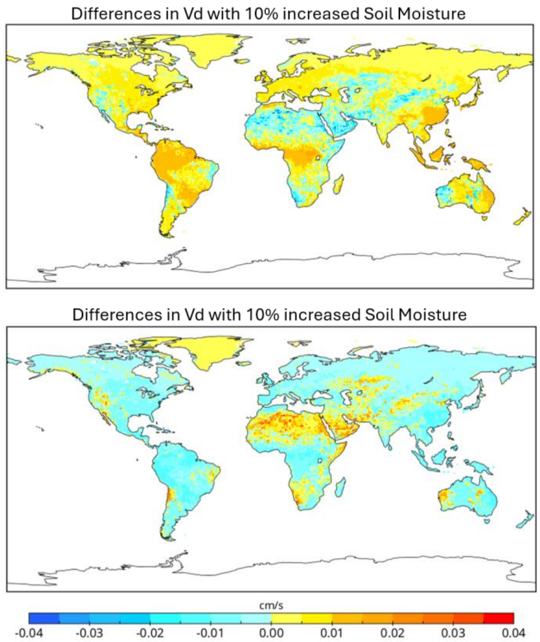

Figure B2. Changes in annual mean H_2 dry deposition velocity (cm s^{-1}) in response to ±10 % soil moisture perturbation.

https://doi.org/10.5194/egusphere-2026-5371
Preprint. Discussion started: 25 September 2026

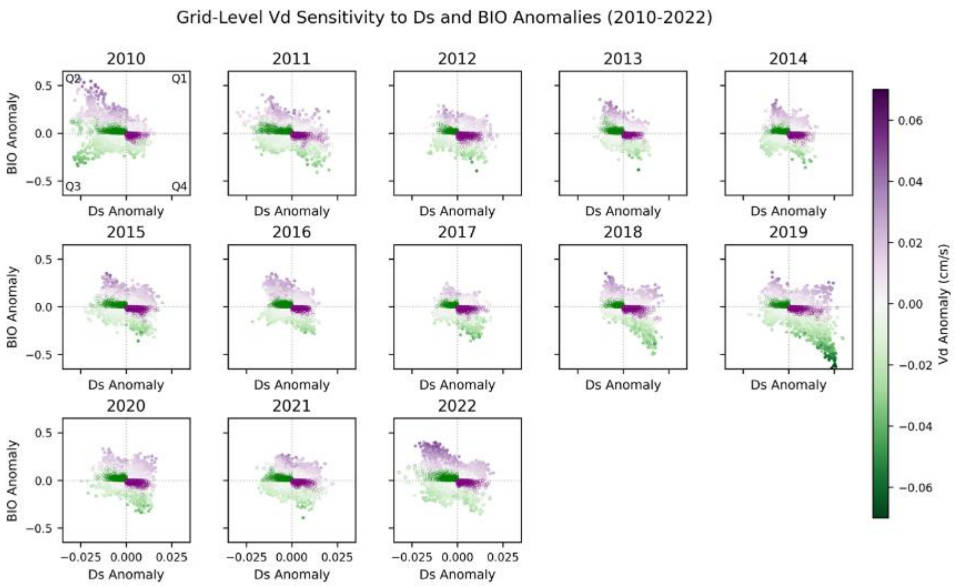

557

558 Figure B3. H_2 deposition velocity anomalies in each model surface grid box (purple: increased Vd; green:
559 decreased Vd) associated with biotic (BIO) and diffusivity (Ds) anomalies each year relative to the long-term
560 mean from 2010 to 2022.

561

https://doi.org/10.5194/egusphere-2026-5371
Preprint. Discussion started: 25 September 2026

Code and data availability

Monthly mean results from control simulation and optimal hydrogen deposition velocity maps can be available soon on Lancaster repository. NOAA Global Monitoring Laboratory H_2 observations can be obtained from https://gml.noaa.gov/ccgg/data/getdata.php?gas=h2, and CAMS anthropogenic, biogenic, and oceanic emissions can be downloaded from https://ads.atmosphere.copernicus.eu/datasets/cams-global-emission-inventories?tab=download or https://eccad.sedoo.fr/#/data. GFAS Biomass burning emissions are available from https://ads.atmosphere.copernicus.eu/datasets/cams-global-fire-emissions-gfas?tab=download. Historical soil parameters from GLDAS are from https://ldas.gsfc.nasa.gov/gldas/soils. CMIP6 model results of future soil parameters were from CEDA archive (https://data.ceda.ac.uk/).

Author contributions

YW and OW designed and conducted this study, and OW provided supervision. YW performed simulations, analysis, and paper writing. OW, XW and RH reviewed and revised the manuscript, and contributed to model development.

Competing interests

The authors declare that they have no conflict of interest.

Acknowledgement

We gratefully acknowledge the organisations and research communities that developed and made available the observational and emissions datasets used in this study. We acknowledge NOAA for providing H_2 observations, Copernicus Atmosphere Monitoring Service (2020) (DOI: 10.24381/1d158bec) for providing CAMS emission inventories, NASA Goddard Earth Sciences Data and Information Services Center (GES DISC) for providing GLDAS soil data, and the CMIP6 project for providing future projected data of soil parameters.

Financial support

This work was funded by UK Research and Innovation (UKRI) under the UK government's Horizon Europe funding Guarantee [10089618], as a contribution to HYDRA (Hydrogen economy benefits and Risks: tools development and policies implementation to mitigate possible climate impacts), Horizon Europe project number 101137758.

https://doi.org/10.5194/egusphere-2026-5371
Preprint. Discussion started: 25 September 2026

References

Aranjuelo, I., Molero, G., Erice, G., Avice, J. C., and Nogués, S.: Plant physiology and proteomics reveals the leaf response to drought in alfalfa (Medicago sativa L.), Journal of Experimental Botany, 62, 111-123, https://doi.org/10.1093/jxb/erq249, 2011.

Bertagni, M. B., Paulot, F., and Porporato, A.: Moisture fluctuations modulate abiotic and biotic limitations of H2 soil uptake, Global Biogeochemical Cycles, 35, e2021GB006987, https://doi.org/10.1029/2021GB006987, 2021.

Boucher, O., Denvil, S., Levavasseur, G., Cozic, A., Caubel, A., Foujols, M.-A., Meurdesoif, Y., Cadule, P., Devilliers, M., Ghattas, J., Lebas, N., Lurton, T., Mellul, L., Musat, I., Mignot, J., and Cheruy, F.: IPSL IPSL-CM6A-LR model output prepared for CMIP6 CMIP historical, Earth System Grid Federation [dataset], 10.22033/ESGF/CMIP6.5195, 2018.

Brown, M. A. J., Warwick, N. J., and Archibald, A. T.: Multi-model assessment of future hydrogen soil deposition and lifetime using CMIP6 data, Geophysical Research Letters, 52, e2024GL113653, https://doi.org/10.1029/2024GL113653, 2025.

Brown, M. A. J., Warwick, N. J., Abraham, N. L., Griffiths, P. T., Rumbold, S. T., Folberth, G. A., O'Connor, F. M., Bryant, H., and Archibald, A. T.: Development of fully interactive hydrogen with methane in UKESM1.0, Geoscientific Model Development, 19, 1537-1557, https://doi.org/10.5194/gmd-19-1537-2026, 2026.

Bryant, H. N., Stevenson, D. S., Heal, M. R., and Abraham, N. L.: Impacts of hydrogen on tropospheric ozone and methane and their modulation by atmospheric NOx, Frontiers in Energy Research, Volume 12 - 2024, https://doi.org/10.3389/fenrg.2024.1415593, 2024.

Cook, B. I., Mankin, J. S., Marvel, K., Williams, A. P., Smerdon, J. E., and Anchukaitis, K. J.: Twenty-first century drought projections in the CMIP6 forcing scenarios, Earth's Future, 8, e2019EF001461, https://doi.org/10.1029/2019EF001461, 2020.

Derwent, R. G., Collins, W. J., Johnson, C. E., and Stevenson, D. S.: Transient behaviour of tropospheric ozone precursors in a Global 3-D CTM and their indirect greenhouse effects, Climatic Change, 49, 463-487, https://doi.org/10.1023/A:1010648913655, 2001.

Derwent, R. G., Stevenson, D. S., Utembe, S. R., Jenkin, M. E., Khan, A. H., and Shallcross, D. E.: Global modelling studies of hydrogen and its isotopomers using STOCHEM-CRI: Likely radiative forcing consequences of a future hydrogen economy, International Journal of Hydrogen Energy, 45, 9211-9221, https://doi.org/10.1016/j.ijhydene.2020.01.125, 2020.

Drewer, J., Cowan, N., Bezanger, A., Hanlon, M., Roberts, T., Karbin, S., Devlin, R., Tweedie, A., Nalavade, R., and Nemitz, E.: Characterizing environmental drivers of the soil hydrogen sink through controlled laboratory experiments, Geoderma, 469, 117803, https://doi.org/10.1016/j.geoderma.2026.117803, 2026.

Ehhalt, D. H. and Rohrer, F.: The tropospheric cycle of H2: a critical review, Tellus B: Chemical and Physical Meteorology, 61, 500-535, https://doi.org/10.1111/j.1600-0889.2009.00416.x, 2009.

Ehhalt, D. H. and Rohrer, F.: Deposition velocity of H2: a new algorithm for its dependence on soil moisture and temperature, Tellus B: Chemical and Physical Meteorology, https://doi.org/10.3402/tellusb.v65i0.19904, 2013.

Fahrin, F., Jones, D. C., Wu, Y., Keeble, J., and Archibald, A. T.: Technical note: Unsupervised classification of ozone profiles in UKESM1, Atmospheric Chemistry and Physics, 23, 3609-3627, https://doi.org/10.5194/acp-23-3609-2023, 2023.

Field, R. A. and Derwent, R. G.: Global warming consequences of replacing natural gas with hydrogen in the domestic energy sectors of future low-carbon economies in the United Kingdom and the United States of America,

https://doi.org/10.5194/egusphere-2026-5371
Preprint. Discussion started: 25 September 2026

International Journal of Hydrogen Energy, 46, 30190-30203, https://doi.org/10.1016/j.ijhydene.2021.06.120, 2021.

Flynn, B., Graham, A., Scott, N., Layzell, D. B., and Dong, Z.: Nitrogen fixation, hydrogen production and N2O emissions, Canadian Journal of Plant Science, 94, 1037-1041, https://doi.org/10.4141/cjps2013-210, 2014.

Fontrodona Bach, A., van der Schrier, G., Melsen, L. A., Klein Tank, A. M. G., and Teuling, A. J.: Widespread and accelerated decrease of observed mean and extreme snow depth over Europe, Geophysical Research Letters, 45, 12,312-312,319, https://doi.org/10.1029/2018GL079799, 2018.

Gottschalck, J., Meng, J., Rodell, M., and Houser, P.: Analysis of multiple precipitation products and preliminary assessment of their impact on Global Land Data Assimilation System Land Surface States, Journal of Hydrometeorology, 6, 573-598, http://www.jstor.org/stable/24910074, 2005.

Granier, C., Lamarque, J., Mieville, A., Muller, J., Olivier, J., Orlando, J., Peters, J., Petron, G., Tyndall, G., and Wallens, S.: POET, a database of surface emissions of ozone precursors [dataset], 2005.

Hammer, S. and Levin, I.: Seasonal variation of the molecular hydrogen uptake by soils inferred from continuous atmospheric observations in Heidelberg, southwest Germany, Tellus B: Chemical and Physical Meteorology, 61, 556-565, https://doi.org/10.1111/j.1600-0889.2009.00417.x, 2009.

International Energy Agency: Global Hydrogen Review 2024, International Energy Agency, Paris, https://www.iea.org/reports/global-hydrogen-review-2024, 2024.

Jordaan, K., Lappan, R., Dong, X., Aitkenhead Ian, J., Bay Sean, K., Chiri, E., Wieler, N., Meredith Laura, K., Cowan Don, A., Chown Steven, L., and Greening, C.: Hydrogen-oxidizing bacteria are abundant in desert soils and strongly stimulated by hydration, mSystems, 5, 10.1128/msystems.01131-01120, https://doi.org/10.1128/msystems.01131-20, 2020.

Kohl, D. H., Kennelly, E. J., Zhu, Y., Schubert, K. R., and Shearer, G.: Proline accumulation, iitrogenase (C2H2 reducing) activity and activities of enzymes related to proline metabolism in drought-stressed soybean nodules, Journal of Experimental Botany, 42, 831-837, https://doi.org/10.1093/jxb/42.7.831, 1991.

Lallo, M., Aalto, T., Laurila, T., and Hatakka, J.: Seasonal variations in hydrogen deposition to boreal forest soil in southern Finland, Geophysical Research Letters, 35, https://doi.org/10.1029/2007GL032357, 2008.

Makar, P. A., Akingunola, A., Aherne, J., Cole, A. S., Aklilu, Y. A., Zhang, J., Wong, I., Hayden, K., Li, S. M., Kirk, J., Scott, K., Moran, M. D., Robichaud, A., Cathcart, H., Baratzedah, P., Pabla, B., Cheung, P., Zheng, Q., and Jeffries, D. S.: Estimates of exceedances of critical loads for acidifying deposition in Alberta and Saskatchewan, Atmospheric Chemistry and Physics, 18, 9897-9927, https://doi.org/10.5194/acp-18-9897-2018, 2018.

Meredith, L. K., Commane, R., Keenan, T. F., Klosterman, S. T., Munger, J. W., Templer, P. H., Tang, J., Wofsy, S. C., and Prinn, R. G.: Ecosystem fluxes of hydrogen in a mid-latitude forest driven by soil microorganisms and plants, Global Change Biology, 23, 906-919, https://doi.org/10.1111/gcb.13463, 2017.

Novelli, P. C., Lang, P. M., Masarie, K. A., Hurst, D. F., Myers, R., and Elkins, J. W.: Molecular hydrogen in the troposphere: Global distribution and budget, Journal of Geophysical Research: Atmospheres, 104, 30427-30444, https://doi.org/10.1029/1999JD900788, 1999.

O'Connor, F. M., Johnson, B. T., Jamil, O., Andrews, T., Mulcahy, J. P., and Manners, J.: Apportionment of the pre-industrial to present-day climate forcing by methane using UKESM1: The role of the cloud radiative effect, Journal of Advances in Modeling Earth Systems, 14, e2022MS002991, https://doi.org/10.1029/2022MS002991, 2022.

Ouyang, Z., Jackson, R. B., Saunois, M., Canadell, J. G., Zhao, Y., Morfopoulos, C., Krummel, P. B., Patra, P. K., Peters, G. P., Dennison, F., Gasser, T., Archibald, A. T., Arora, V., Baudoin, G., Chandra, N., Ciais, P., Davis, S.

https://doi.org/10.5194/egusphere-2026-5371
Preprint. Discussion started: 25 September 2026

J., Feron, S., Guo, F., Hauglustaine, D., Jones, C. D., Jones, M. W., Kato, E., Kennedy, D., Knauer, J., Lienert, S., Lombardozzi, D., Melton, J. R., Nabel, J. E. M. S., O'Sullivan, M., Pétron, G., Poulter, B., Rogelj, J., Sandoval Calle, D., Smith, P., Suntharalingam, P., Tian, H., Wang, C., and Wiltshire, A.: The global hydrogen budget, Nature, 648, 616-624, https://doi.org/10.1038/s41586-025-09806-1, 2025.

Patterson, J. D., Aydin, M., Crotwell, A. M., Petron, G., Severinghaus, J. P., and Saltzman, E. S.: Atmospheric history of H_2 over the past century reconstructed from South Pole firn air, Geophysical Research Letters, 47, e2020GL087787, https://doi.org/10.1029/2020GL087787, 2020.

Paulot, F., Pétron, G., Crotwell, A. M., and Bertagni, M. B.: Reanalysis of NOAA H_2 observations: implications for the H_2 budget, Atmospheric Chemistry and Physics, 24, 4217-4229, https://doi.org/10.5194/acp-24-4217-2024, 2024.

Paulot, F., Paynter, D., Naik, V., Malyshev, S., Menzel, R., and Horowitz, L. W.: Global modeling of hydrogen using GFDL-AM4.1: Sensitivity of soil removal and radiative forcing, International Journal of Hydrogen Energy, 46, 13446-13460, https://doi.org/10.1016/j.ijhydene.2021.01.088, 2021.

Pétron, G., Crotwell, A. M., Mund, J., Crotwell, M., Mefford, T., Thoning, K., Hall, B., Kitzis, D., Madronich, M., Moglia, E., Neff, D., Wolter, S., Jordan, A., Krummel, P., Langenfelds, R., and Patterson, J.: Atmospheric H_2 observations from the NOAA Cooperative Global Air Sampling Network, Atmospheric Measurement Techniques, 17, 4803-4823, https://doi.org/10.5194/amt-17-4803-2024, 2024.

Pinzer, B. R., Kerbrat, M., Huthwelker, T., Gäggeler, H. W., Schneebeli, M., and Ammann, M.: Diffusion of NO_x and HONO in snow: A laboratory study, Journal of Geophysical Research: Atmospheres, 115, https://doi.org/10.1029/2009JD012459, 2010.

Prather, M. J., Holmes, C. D., and Hsu, J.: Reactive greenhouse gas scenarios: Systematic exploration of uncertainties and the role of atmospheric chemistry, Geophysical Research Letters, 39, https://doi.org/10.1029/2012GL051440, 2012.

Price, H., Jaeglé, L., Rice, A., Quay, P., Novelli, P. C., and Gammon, R.: Global budget of molecular hydrogen and its deuterium content: Constraints from ground station, cruise, and aircraft observations, Journal of Geophysical Research: Atmospheres, 112, https://doi.org/10.1029/2006JD008152, 2007.

Qiao, D., Li, Z., Zeng, J., Liang, S., McColl, K. A., Bi, H., Zhou, J., and Zhang, P.: Uncertainty characterization of ground-based, satellite, and reanalysis snow depth products using extended triple collocation, Water Resources Research, 58, e2021WR030895, https://doi.org/10.1029/2021WR030895, 2022.

Rhee, T. S., Brenninkmeijer, C. A. M., and Röckmann, T.: The overwhelming role of soils in the global atmospheric hydrogen cycle, Atmospheric Chemistry and Physics, 6, 1611-1625, https://doi.org/10.5194/acp-6-1611-2006, 2006.

Richards, L. C., Davey, N. G., Gill, C. G., and Krogh, E. T.: Discrimination and geo-spatial mapping of atmospheric VOC sources using full scan direct mass spectral data collected from a moving vehicle, Environmental Science: Processes & Impacts, 22, 173-186, https://doi.org/10.1039/c9em00439d, 2020.

Ryan, E., Wild, O., Voulgarakis, A., and Lee, L.: Fast sensitivity analysis methods for computationally expensive models with multi-dimensional output, Geoscientific Model Development, 11, 3131-3146, https://doi.org/10.5194/gmd-11-3131-2018, 2018.

Salstein, D. A., Ponte, R. M., and Cady-Pereira, K.: Uncertainties in atmospheric surface pressure fields from global analyses, Journal of Geophysical Research: Atmospheres, 113, https://doi.org/10.1029/2007JD009531, 2008.

Saltelli, A., Tarantola, S., Campolongo, F., and Ratto, M.: Sensitivity analysis in practice: a guide to assessing scientific models, Wiley Online Library, Chichester, UK, https://doi.org/10.1002/0470870958, 2004.

https://doi.org/10.5194/egusphere-2026-5371
Preprint. Discussion started: 25 September 2026

Saltelli, A., Annoni, P., Azzini, I., Campolongo, F., Ratto, M., and Tarantola, S.: Variance based sensitivity analysis of model output. Design and estimator for the total sensitivity index, Computer physics communications, 181, 259-270, https://doi.org/10.1016/j.cpc.2009.09.018, 2010.

Sand, M., Skeie, R. B., Sandstad, M., Krishnan, S., Myhre, G., Bryant, H., Derwent, R., Hauglustaine, D., Paulot, F., Prather, M., and Stevenson, D.: A multi-model assessment of the Global Warming Potential of hydrogen, Communications Earth & Environment, 4, 203, https://doi.org/10.1038/s43247-023-00857-8, 2023.

Smith-Downey, N. V., Randerson, J. T., and Eiler, J. M.: Temperature and moisture dependence of soil H2 uptake measured in the laboratory, Geophysical Research Letters, 33, https://doi.org/10.1029/2006GL026749, 2006.

Sobol′, I. M.: Global sensitivity indices for nonlinear mathematical models and their Monte Carlo estimates, Mathematics and Computers in Simulation, 55, 271-280, https://doi.org/10.1016/S0378-4754(00)00270-6, 2001.

Song, T., Wang, J., Yu, X., and de Leeuw, G.: Application of Gaussian Mixture Models for aerosol type analysis in China, Atmospheric Research, 294, 106938, https://doi.org/10.1016/j.atmosres.2023.106938, 2023.

Spennemann, P. C., Fernández-Long, M. E., Gattinoni, N. N., Cammalleri, C., and Naumann, G.: Soil moisture evaluation over the Argentine Pampas using models, satellite estimations and in-situ measurements, Journal of Hydrology: Regional Studies, 31, 100723, https://doi.org/10.1016/j.ejrh.2020.100723, 2020.

Stroo, F. T., Hooghiem, J. J. D., Krol, M. C., and Peters, W.: Constraining the hydrogen soil sink and photochemical source: Insights from atmospheric H_2 Inversions (2003–2023), EGUsphere, 2026, 1-43, https://doi.org/10.5194/egusphere-2026-3077, 2026.

Sturm, M., Holmgren, J., and Liston, G. E.: A seasonal snow cover classification system for local to global applications, Journal of Climate, 8, 1261-1283, https://doi.org/10.1175/1520-0442(1995)008<1261:ASSCCS>2.0.CO;2, 1995.

Surawski, N., Steil, B., Brühl, C., Gromov, S., Klingmüller, K., Martin, A., Pozzer, A., and Lelieveld, J.: Global atmospheric hydrogen chemistry and source-sink budget equilibrium simulation with the EMAC v2.55 model, Geoscientific Model Development, 19, 911-931, https://doi.org/10.5194/gmd-19-911-2026, 2026.

Tian, F., Zhang, R.-H., Liu, C., and Guan, C.: Rainfall sustains multiyear La Niña, Nature Communications, 17, 1744, https://doi.org/10.1038/s41467-026-68451-y, 2026.

Trapani, D., Marocco, P., Gandiglio, M., and Santarelli, M.: Hydrogen leakages across the supply chain: Current estimates and future scenarios, International Journal of Hydrogen Energy, 145, 1084-1095, https://doi.org/10.1016/j.ijhydene.2025.06.103, 2025.

Tromp, T. K., Shia, R.-L., Allen, M., Eiler, J. M., and Yung, Y. L.: Potential environmental impact of a hydrogen economy on the stratosphere, Science, 300, 1740-1742, https://doi.org/10.1126/science.1085169, 2003.

Wang, H., van Eyk, P. J., Medwell, P. R., Birzer, C. H., Tian, Z. F., Possell, M., and Huang, X.: Air permeability of the litter layer in broadleaf forests, Frontiers in Mechanical Engineering, Volume 5 - 2019, https://doi.org/10.3389/fmech.2019.00053, 2019.

Warwick, N. J., Bekki, S., Nisbet, E. G., and Pyle, J. A.: Impact of a hydrogen economy on the stratosphere and troposphere studied in a 2-D model, Geophysical Research Letters, 31, https://doi.org/10.1029/2003GL019224, 2004.

Warwick, N. J., Archibald, A. T., Griffiths, P. T., Keeble, J., O'Connor, F. M., Pyle, J. A., and Shine, K. P.: Atmospheric composition and climate impacts of a future hydrogen economy, Atmospheric Chemistry and Physics, 23, 13451-13467, https://doi.org/10.5194/acp-23-13451-2023, 2023.

https://doi.org/10.5194/egusphere-2026-5371
Preprint. Discussion started: 25 September 2026

Wild, O.: Modelling the global tropospheric ozone budget: exploring the variability in current models, Atmospheric Chemistry and Physics, 7, 2643-2660, https://doi.org/10.5194/acp-7-2643-2007, 2007.

Wild, O. and Ryan, E. M.: Quantifying and addressing the uncertainties in tropospheric ozone and OH in a global chemistry transport model, Atmospheric Chemistry and Physics, 26, 2255-2273, https://doi.org/10.5194/acp-26-2255-2026, 2026.

Yang, L. H., Jacob, D. J., Lin, H., Dang, R., Bates, K. H., East, J. D., Travis, K. R., Pendergrass, D. C., and Murray, L. T.: Assessment of hydrogen's climate impact is affected by model OH Biases, Geophysical Research Letters, 52, e2024GL112445, https://doi.org/10.1029/2024GL112445, 2025.

Yashiro, H., Sudo, K., Yonemura, S., and Takigawa, M.: The impact of soil uptake on the global distribution of molecular hydrogen: chemical transport model simulation, Atmospheric Chemistry and Physics, 11, 6701-6719, https://doi.org/10.5194/acp-11-6701-2011, 2011.

Yonemura, S., Yokozawa, M., Kawashima, S., and Tsuruta, H.: Model analysis of the influence of gas diffusivity in soil on CO and H2 uptake, Tellus B: Chemical and Physical Meteorology, https://doi.org/10.3402/tellusb.v52i3.17075, 2000.

Zhao, C., Gong, C., Duan, H., Yan, P., Liu, Y., and Zhou, G.: Evaluation of three reanalysis soil temperature datasets with observation data over China, Earth, 3, 1042-1058, https://doi.org/10.3390/earth3040060, 2022a.

Zhao, L., Yang, K., He, J., Zheng, H., and Zheng, D.: Potential of mapping global soil texture type from SMAP soil moisture product: A pilot study, IEEE Transactions on Geoscience and Remote Sensing, 60, 1-10, https://doi.org/10.1109/TGRS.2021.3119667, 2022b.

Zhu, T., Yu, J.-Y., and Lo, M.-H.: Amplified impacts of multi-year La Niñas on soil moisture compared to single-year La Niñas, npj Climate and Atmospheric Science, 8, 301, https://doi.org/10.1038/s41612-025-01175-w, 2025.